JOURNAL OF SOLID STATE CHEMISTRY **131,** 160–166 (1997)
ARTICLE NO. SC977390

Synthesis and Characterizations of a Polymorphic Sodium Cobalt Phosphate with Edge-Sharing Co^{2+} Octahedral Chains

Pingyun Feng, Xianhui Bu, and Galen D. Stucky

Chemistry Department, University of California, Santa Barbara, California 93106

Received July 19, 1996; in revised form November 21, 1996; accepted March 12, 1997

A new sodium cobalt phosphate with a three-dimensional framework structure has been prepared by the hydrothermal method and characterized by thermal analysis, susceptibility measurements, and single crystal X-ray diffraction. The oxide framework is built from octahedral and tetrahedral atoms (Co^{2+} and P^{5+}) and consists of cross-linked infinite Co–O–Co chains that propagate along the crystallographic *b*-axis. The framework connectivity can be correlated to that of potassium titanyl phosphate (KTP) type structure. The structure of $NaCoPO_4$ is also compared to other divalent metal phosphates and a summary of structures isotypic to $NaCoPO_4$ is given. Magnetic susceptibility measurements show that the compound displays Curie–Weiss behavior down to a temperature of 13 K at which an antiferromagnetic phase transition occurs. The thermal analysis shows that the octahedral polymorph is a product of a phase transformation of the trigonal bipyramidal polymorph at about 710°C. The octahedral polymorph transforms into the tetrahedral polymorph at about 920°C. Crystal data for $NaCoPO_4$: $M = 176.89$, space group *Pnma* (No. 62), $a = 8.8957(12)$, $b = 6.8007(9)$, $c = 5.0341(7)$, $V = 304.55(7)$ Å^3, $Z = 4$, $D_c = 3.858\ g\,cm^{-3}$, pink thin plate, Mo$K\alpha$, $\lambda = 0.71073$ Å, $\mu = 6.128\ mm^{-1}$, $2\theta_{max} = 56.38°$, $R(F) = 3.68\%$ for 41 parameters and 328 reflections with $I > 2\sigma(I)$. © 1997 Academic Press

INTRODUCTION

Cobalt framework structures are of interest for several reasons. Phosphates of the type $M^{I}M^{II}PO_4$, where M^{I} stands for a monovalent cation and M^{II} for a divalent cation are known to show ferroic properties and are extensively studied (1, 2). A number of open framework materials with only a partial incorporation of cobalt ions into the framework sites have been demonstrated to have catalytic properties (3, 4).

In this paper, we report a new sodium cobalt phosphate with a three-dimensional framework consisting of octahedral (Co^{2+}) and tetrahedral centers (P^{5+}) in a ratio of 1. The framework can be correlated to that of the well known KTP-type structure (KTP, potassium titanyl phosphate) (5). The differences between $NaCoPO_4$ and the KTP-type structures result from the need to accommodate lower charged octahedral centers (Co^{2+} in this case) in the cobalt compound. The framework connectivity of the octahedral–tetrahedral cobalt phosphate structure results in a $ABCO_4$ stoichiometry as compared to the KTP–type framework which has a $ABCO_5$ stoichiometry.

Oxides built from octahedral and tetrahedral centers are an important class of materials. In addition to KTP-type structures which show nonlinear optical properties and are used commercially for second harmonic generation (5), other octahedral–tetrahedral oxides with spinel or garnet structures have ferrimagnetic properties which are used in commercial applications such as magnetic recordings (6).

EXPERIMENTAL

Hydrothermal Synthesis

$CoCO_3 \cdot xH_2O$ (0.56 g) was mixed with distilled water (8.64 g). Carbon dioxide evolved when 1.21 g of 85% H_3PO_4 was slowly added to the above mixture. With stirring, 1.13 g of $(CH_3)_2NH$ (40 wt% solution in water) and 2.05 g of 6 *M* NaOH solution were added. The color of the gel changed from pink to blue. The mixture was then heated at 180°C for 3 days in a Teflon coated steel autoclave. The product was recovered by filtration and washed with deionized water. Translucent pale pink plate-like crystals were obtained together with a nearly equal amount of dark red needle-like crystals. The two different phases could be easily separated since crystals of the same phase grew into star-like clusters. They were identified as two different polymorphs of $NaCoPO_4$ by single crystal X-ray diffraction. The dark red phase consists of Co^{2+} in the trigonal bipyramidal coordination (7) whereas the pink crystal consists of octahedrally coordinated Co^{2+}. The structure and magnetic properties of the pink phase are reported below.

Thermal Analysis

The as-synthesized sample (49.5 mg) consisting of both red and pink phases was used for thermogravimetric analysis

0022-4596/97 $25.00

(TG) and differential thermal analysis (DTA), which were performed on a Netzsch Simultaneous Thermal Analysis (STA) 409 system in static air with a heating rate of 5°C/min from 30 to 1000°C. There was no weight change throughout the measured temperature range. However, there were an endothermic event occurring at about 710°C and an exothermic event at about 920°C. As shown below, the endothermic peak corresponded to a phase transition from the red phase to the pink phase and the exothermic peak corresponded to a phase transition from the pink phase to the blue phase. Crystal structures of both red and blue phases have been characterized (7).

Polymorphic Phase Transitions

To help interpret the endothermic and exothermic events shown by the DTA plot, 0.26 g of the as-synthesized crystalline sample consisting of both red and pink phases in about the same volume ratio was placed in a furnace. The temperature of the furnace was programmed to increase from 30 to 825°C within 2 h. The sample was left at 825°C for 30 min and then allowed to cool to room temperature without further temperature control. The microscopic examination of the sample after such a heat treatment showed that the whole sample was highly crystalline and indistinguishable from the starting pink phase. One crystal was examined using single crystal X-ray diffraction and the unit cell parameters found were the same as those obtained from a pink crystal before the heat treatment. This indicated that the pink phase was thermally stable until at least 825°C and the red phase had completely transformed into the pink phase. This was in agreement with the TG and DTA data and was also verified by X-ray powder diffraction which showed the complete disappearance of diffraction peaks from the red phase and presence of diffraction peaks from the pink phase.

The above sample which had been treated at 825°C was put back in a furnace and the temperature of the furnace was programmed to increase from 30 to 925°C within 3 h. The sample was left at 925°C for 3 h and then allowed to cool to room temperature without further temperature control. The microscopic examination showed that the whole sample had turned into the crystalline blue phase. This was in agreement with the TG and DTA data. The blue phase was also verified by X-ray powder diffraction.

Powder Diffraction

The powder diffraction data were obtained on a Scintag PAD-X automated diffractometer operating in θ–θ geometry with a Ge solid state detector and Cu$K\alpha$ radiation. The data were collected from 3° to 60° with a step size of 0.03° and a counting time of 2 s per step.

Magnetic Susceptibility

Susceptibility measurements were carried out using a Quantum Design MPMS-5S Magnetic Properties Measuring System with a sample weight of 8.7 mg. The polycrystalline sample was obtained by grinding hand-picked crystals. The phase identity was checked by X-ray powder diffraction. The measurements of the field dependence were carried out at temperatures of 1.7 and 5 K. The measurements of the temperature dependence were made from 1.7 to 300 K in an applied field of 250 G for the sample cooled in zero field and 250 G field, respectively.

Single Crystal Structure Determination

One crystal of the pale pink $NaCoPO_4$ was glued to a thin glass fibre with epoxy resin and mounted on a Siemens Smart CCD diffractometer equipped with a normal focus, 2.4 kW sealed tube X-ray source (Mo$K\alpha$ radiation, $\lambda = 0.71073$ Å) operating at 50 kV and 40 mA. About 1.3 hemisphere of intensity data were collected in 1321 frames with ω scans (width of 0.30° and exposure time of 30 s per frame). Unit cell dimensions were determined by a least-squares fit of 995 reflections with $I > 10\sigma(I)$ and $10° < 2\theta < 56°$. The empirical absorption correction was based on the equivalent reflections, and other possible effects such as the absorption by the glass fibre were simultaneously corrected. The structure was solved by Patterson methods followed by successive difference Fourier methods. All calculations were performed using SHELXTL running

TABLE 1
Summary of Crystal Data and Refinement Results

Structural formula	$NaCoPO_4$
Formula weight	176.89
Color and habit	Pink thin plate
Crystal size (mm^3)	$0.28 \times 0.16 \times 0.04$
a(Å)	8.896(1)
b(Å)	6.8007(9)
c(Å)	5.0341(7)
V(Å^3)	305.55(7)
Z	4
Space group	*Pnma* (No. 62)
ρ_{calc} (g/cm^3)	3.858
λ(Mo$K\alpha$) (Å)	0.71073
μ(Mo$K\alpha$) (mm^{-1})	6.128
Maximum 2θ	56.38°
Observed data $I > 2\sigma(I)$	328
Parameters	41
$R(F)^a$	3.68%
$R_w(F^2)^b$	9.43%
GOF	1.15

[a] $R(F) = \sum||F_o| - |F_c||/\sum|F_o|$ with $F_o > 4.0\ \sigma(F)$.
[b] $R_w(F^2) = [\sum[w(F_o^2 - F_c^2)^2]/\sum[w(F_o^2)^2]]^{1/2}$ with $F_o > 4.0\sigma(F)$. $w = 1/[\sigma^2(F_o^2) + (0.0612P)^2]$, where $P = (F_o^2 + 2F_c^2)/3$.

TABLE 2
Atomic Coordinates ($\times 10^4$) and Equivalent Isotropic Displacement Parameters ($Å^2 \times 10^3$)

	x	*y*	*z*	*U*(eq)
Co(1)	0	0	0	16(1)
P(1)	1775(1)	2500	4630(2)	10(1)
O(1)	1225(2)	661(3)	3164(5)	17(1)
O(2)	1183(3)	2500	7502(6)	14(1)
O(3)	3529(3)	2500	4518(6)	13(1)
Na(1)	3513(2)	2500	9705(4)	17(1)

Note. *U*(eq) is defined as one third of the trace of the orthogonalized U_{ij} tensor.

TABLE 3
Selected Bond Lengths (Å) and Angles (°)

Co(1)–O(1) × 2	1.982(2)	Co(1)–O(2) × 2	2.362(2)
Co(1)–O(3) × 2	2.159(2)	P(1)–O(1) × 2	1.532(2)
P(1)–O(2)	1.538(3)	P(1)–O(3)	1.562(3)
Na(1)–O(1) × 2	2.956(3)	Na(1)–O(1) × 2	2.297(2)
Na(1)–O(1) × 2	2.922(3)	Na(1)–O(2)	2.622(4)
Na(1)–O(2)	2.351(3)	Na(1)–O(3)	2.611(3)
Na(1)–O(3)	2.423(3)		
O(1)–Co(1)–O(1)	180.0	O(1)–Co(1)–O(2)	91.13(9)
O(1)–Co(1)–O(2)	88.87(9)	O(1)–Co(1)–O(3)	93.69(9)
O(1)–Co(1)–O(3)	86.31(9)	O(3)–Co(1)–O(2)	103.71(8)
O(3)–Co(1)–O(2)	76.29(8)	O(2)–Co(1)–O(2)	180.0
O(3)–Co(1)–O(3)	180.0	O(1)–P(1)–O(1)	109.4(2)
O(2)–P(1)–O(3)	112.1(2)	O(1)–P(1)–O(2) × 2	110.08(11)
O(1)–P(1)–O(3) × 2	107.55(11)		

on a Silicon Graphics Indy 5000. Final full-matrix refinements were against F^2 with all reflections and included secondary extinction correction and anisotropic thermal parameters for all atoms. Parameter shifts in the final least-squares cycle were smaller than 0.03σ. The crystallographic results are summarized in Table 1 while the atomic coordinates and selected bond distances are listed in Tables 2 and 3, respectively.

RESULTS AND DISCUSSION

Description of the Framework Connectivity

One interesting feature of the structure is the straight infinite (CoO_4) chains (Fig. 1). $(CoO_4)_\infty$ chains propagate strictly along the cell *b*-axis and are thus perpendicular to the crystallographic mirror plane. The repeat distance (3.400 Å) between the two closest Co^{2+} sites along the chain is only half of the *b*-axis length. This is indicative of the subcell structure of Co^{2+} sites.

The phosphate groups connect pairs of Co^{2+} ions along chains in two different ways (Fig. 2). In one way the phosphate group uses two different oxygen atoms ($-O(PO_2)O-$) to connect two Co^{2+} ions. This gives rise to bi-coordinated oxygen atoms (excluding coordinations to extra framework sodium cations). Each phosphate group uses two of its four oxygen atoms to form such a bridge. This type of bridging is very common and is exclusively found in KTP-type structures.

In the second way, the phosphate group (PO_4^{-3}) uses one oxygen atom ($(PO_3)O^-$) to bridge two Co^{2+} ions. This leads to trigonally coordinated oxygen atoms. There are two such oxygen atoms per phosphate group. As a result, despite the tetrahedral coordination of P^{5+}, each P^{5+} is effectively connected to six Co^{2+} ions. Since each octahedral Co^{2+} is also connected to six P^{5+} tetrahedra, a ratio of 1 for Co/P is obtained (Fig. 3). This type of bridging is

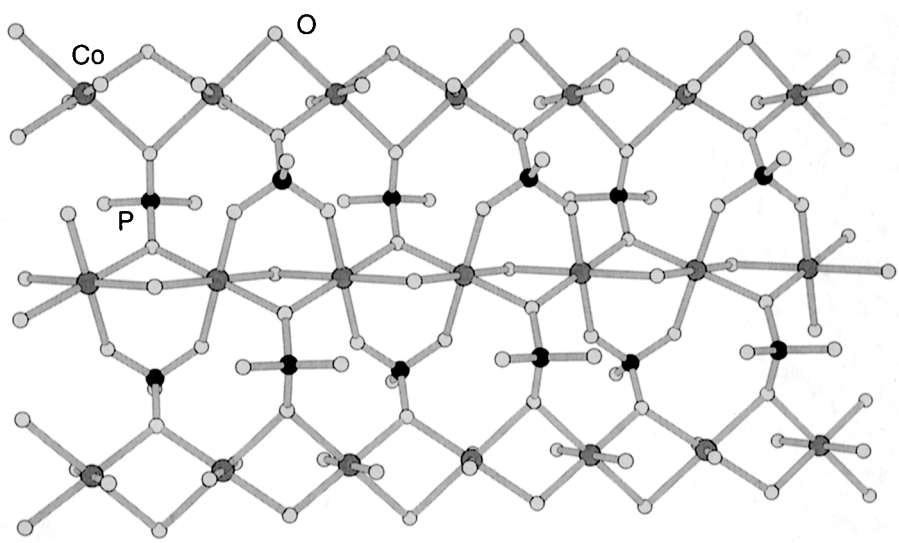

FIG. 1. Three rows of $(CoO_4)_\infty$ chains interconnected by PO_4^{-3} groups.

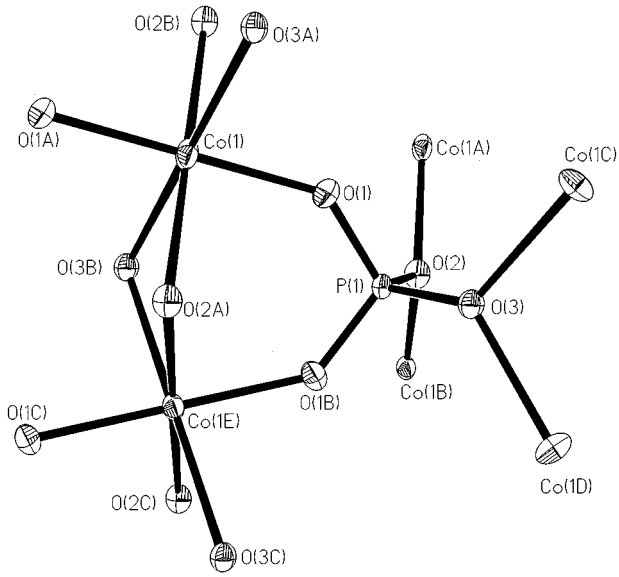

FIG. 2. An ORTEP (50%) drawing showing the local coordination environment. O2 and O3 have trigonal coordinations. The cluster displays mirror symmetry defined by P(1), O(2), and O(3). Atoms with labels containing A, B, … , E are symmetry generated. The asymmetric unit contains only half of the $NaCoPO_4$ formula unit. Co^{2+} octahedra are located on the inversion center while P^{5+} tetrahedra are on the mirror plane. Only O1 is located on the general position.

usually found in phosphates containing octahedral or tetrahedral cations with a low valence. Another example is $[Zn_4(H_2O)(PO_4)_3]$ $NH(CH_3)_3$ (8) in which some oxygen atoms are bonded to two zinc cations and one phosphorous cation.

A projection of the three-dimensional framework is shown in Fig. 4. It consists of small cages where charge balancing sodium ions are located (Fig. 5). The $NaCoPO_4$ framework connectivity serves as a general way of achieving $ABCO_4$-type stoichiometry for an octahedral–tetrahedral oxide framework.

Comparison with the KTP-Type Framework Connectivity

The bridging oxygen atoms in the Co–O–Co linkages are always simultaneously coordinated to P^{5+} tetrahedra. The low valence of Co^{2+} necessitates the trigonal coordination of the bridging oxygen atoms to P^{5+} in order to satisfy the electrostatic valence requirement of the bridging oxygen atoms. However, this is not the case in KTP-type structures where octahedral metal cations have higher valences.

In the KTP-type structure, which is also an octahedral–tetrahedral oxide framework, there is one oxygen atom coordinated only between two metal ions due to the high valence of Ti^{4+}, V^{4+}, or other cations such as Sn^{4+}. This gives one-dimensional vanadyl, titanyl, or other similar chains bridged with phosphate groups. The formation of such metal–oxygen chains leaves only four bonds free on octahedral cations. Therefore each P^{5+} is connected through oxygen bridges to four Ti^{4+}, V^{4+} cations or other octahedral centers and each octahedral cation is connected through oxygen bridges to four P^{5+} ions. This gives a ratio of 1 between tetrahedral sites and octahedral sites. In $NaCoPO_4$, all bridging oxygen atoms between two metal atoms are also part of phosphate groups. So the framework in $NaCoPO_4$ can be considered to consist of rows of discreet Co^{2+} ions bridged by phosphate groups. It can be suggested that the $NaCoPO_4$ framework described here has a modified KTP-type structure. The modification serves to adapt the framework to octahedral metal ions with a low valence.

Other $M^{I}M^{II}PO_4$ Phosphates and Isotypic Structures

A large number of $M^{I}M^{II}PO_4$ phosphates are known (9). These salts can be classified based on the coordination polyhedra of divalent metal cations which can be tetrahedral, octahedral, and five-coordinate. For example, $NaCoPO_4$ has three polymorphs which consist of tetrahedral (the blue phase), trigonal bipyramidal (the red phase), and octahedral (the pink phase) cobalt ions, respectively (7).

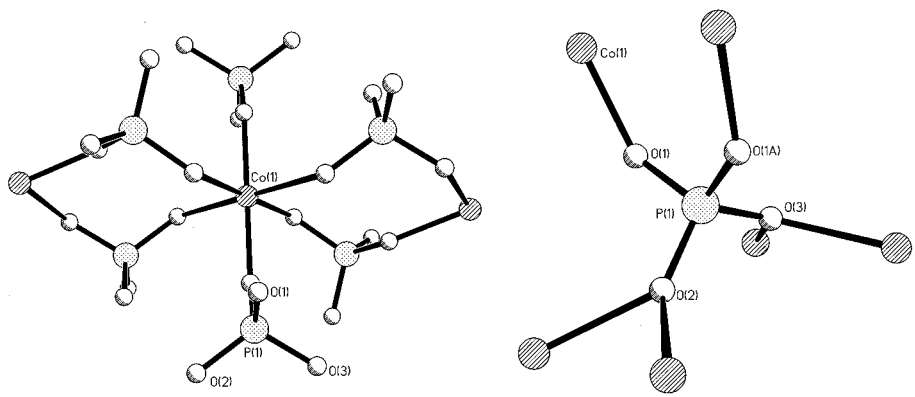

FIG. 3. An illustration of the local connectivity for Co^{2+} and P^{5+} leading to the equal number of Co^{2+} and P^{5+}. PO_4^{-3} can effectively be considered as an octahedral group.

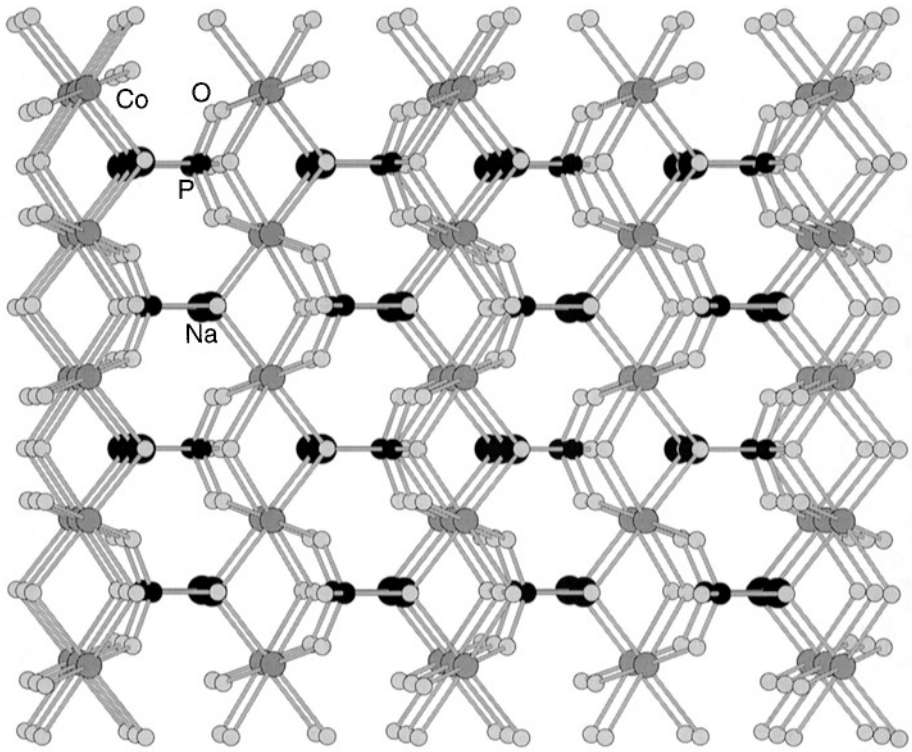

FIG. 4. $NaCoPO_4$ framework viewed down the shortest cell axis (the *c*-axis). Atoms of the same type form columns along this direction except for sodium cations which alternate with trigonal oxygen atoms. Sodium atoms are drawn as unconnected large dark circles. The apparent three bonds to sodium atoms in some cases are actually bonds to oxygen atoms hidden by sodium atoms.

The tetrahedral salts are generally least dense and adopt zeolite *ABW*-type framework topology for large monovalent cations such as NH_4^+, Rb^+, Tl^+, and Cs^+ (10). For smaller cations such as K^+ and sometimes Na^+, a framework topology which can be considered as a hybrid between tridymite and *ABW* frameworks are usually obtained (10). For even smaller cations such as Li^+ and Na^+, the framework topology of phenakite (11), cristobalite (12), and beryllonite (13) often provides better accommodation. When a divalent metal has the increased tendency to adopt higher-than-four coordinations, which is the case for transition metal cations such as Mn, Fe, and Co. (14), they can form nontetrahedral frameworks in the presence of small monovalent cations as an alternative to tetrahedral frameworks such as the phenakite type mentioned above. Such is the case for the pink polymorph of $NaCoPO_4$ described here.

The phase transitions between three different polymorphs of $NaCoPO_4$ involve the breaking and formation of new bonds and are thus reconstructive phase transitions. The phase transition temperatures are significantly higher than $M^{\text{I}}M^{\text{II}}PO_4$ phosphates with large monovalent cations which often show displacive transitions. For example, several $M^{\text{I}}M^{\text{II}}PO_4$ phases have been reported to have displacive phase transitions. The symmetry of the $CsZnPO_4$ *ABW* framework increases with temperature with $P2_1/c$ at room temperature, $Pna2_1$ at 280°C, and *Pnma* at 340°C (15).

The framework topology of $NaCoPO_4$ belongs to the $ZnSO_4$ type. A number of ternary salts have been known to have such a framework structure (Table 4). In these structures, the cages similar to those occupied by sodium cations in $NaCoPO_4$ are empty (16). In quarternary structures, only small extra-framework cations such as sodium are found to reside in these cages. A list of isotypic structures, both ternary and quarternary, are presented in Table 4.

Magnetic Properties

The temperature dependence of magnetic susceptibility data for the sample cooled in zero field is shown in Fig. 6. The temperature dependence for the sample cooled in 250 G field shows the same behavior. The field dependence of magnetization is shown in Fig. 7. Since there is very little difference between 1.7 and 5 K data, only the field dependence data at 1.7 K is shown. The susceptibility data exhibit Curie–Weiss paramagnetism down to a temperature of 13 K at which the sample turns antiferromagnetic. Thus the maximum in the magnetic susceptibility is observed at

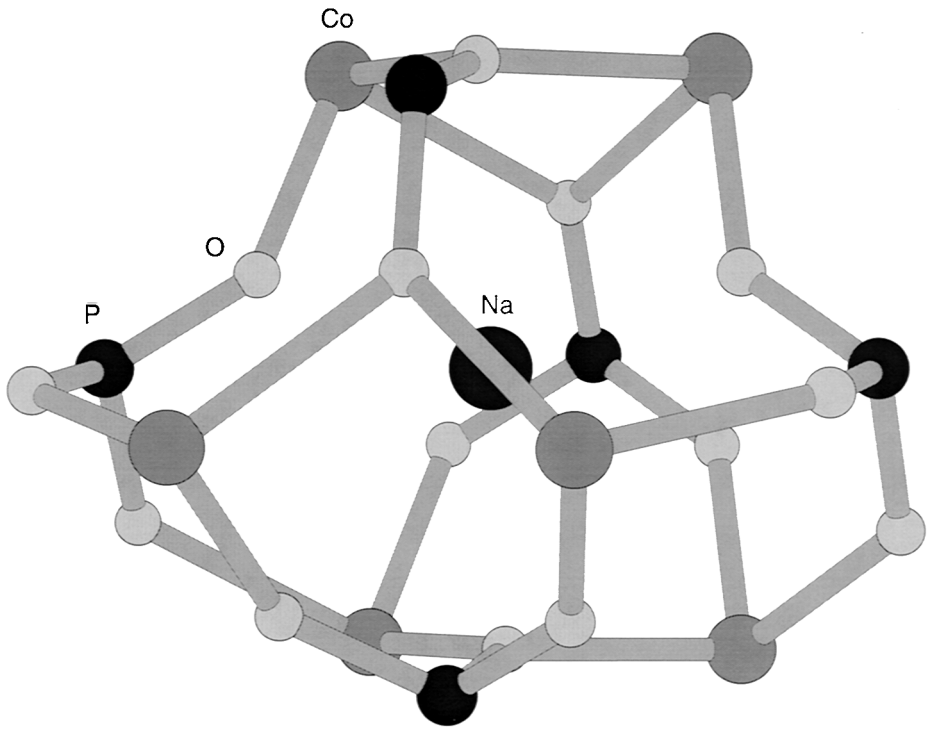

FIG. 5. Illustration of the local coordination environment for a sodium atom inside a cage.

13 K. A linear curve fit to the Curie–Weiss law gives $C = 2.508$ emu K/mol, $\theta = -19.5$ K. This gives a magnetic moment of 4.48 μ_B, which is smaller than the magnetic moments typically observed for octahedral Co^{2+} ions (4.7–5.2 μ_B) (17). The smaller magnetic moment is likely to be a result of the octahedral distortion as evidenced by three pairs of significantly different Co–O bond distances ranging from 1.982(2) to 2.362(2) Å. For three unpaired electrons, the g value is calculated to be 2.31.

The $M(H)$ behavior shows that there is a phase transition at a critical field of 4×10^{-4} G. It appears that the antiferromagnetic spin alignment is disrupted due to the high applied field and the new phase is likely to be a nonordered paramagnetic state.

TABLE 4
A Summary of Compounds Isotypic to $NaCoPO_4$

Compounds	Space group	*a*	*b*	*c*
$ZnSO_4$ (18, 19)	*Pnma*	8.604(5)	6.746(5)	4.774(3)
$CoSO_4$ (20)	*Pnma*	8.613	6.706	4.740
$MgSO_4$ (16)	*Pnma*	8.575	6.699	4.742
$CuSO_4$ (21)	*Pnma*	8.390	6.690	4.830
$CoSeO_4$ (22)	*Pnma*	9.047(3)	6.750(2)	4.891(1)
$MnSeO_4$ (22)	*Pnma*	9.219(3)	7.027(2)	4.960(2)
$MgSeO_4$ (23)	*Pnma*	9.001(6)	6.741(4)	4.903(4)
$CrAsO_4$ (24)	*Pnma*	8.995(2)	6.237(3)	4.755(1)
$NaCoPO_4$	*Pnma*	8.896(1)	6.8007(9)	5.0341(7)
$NaMnPO_4$ (25)	*Pnma*	9.088	6.904	5.113
$Na(Fe,Zn)PO_4$ (26)	*Pnma*	8.972(5)	6.854(3)	5.031(1)
$Na(Fe_{0.9})PO_4$ (27)	*Pnma*	8.987(1)	6.861(1)	5.045(1)

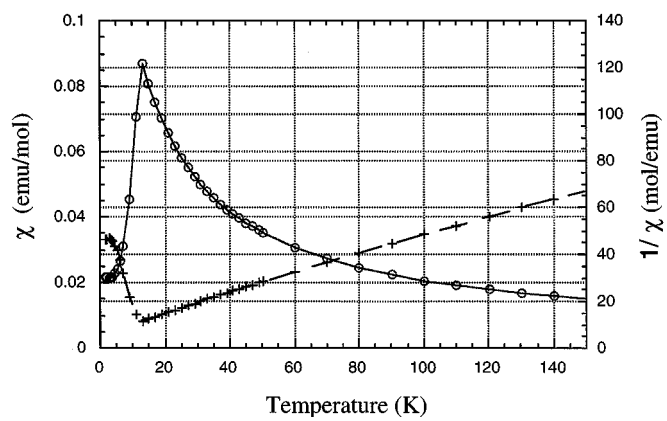

FIG. 6. Molar susceptibility and inverse molar susceptibility plotted as a function of temperature over the 1.7–150 K region.

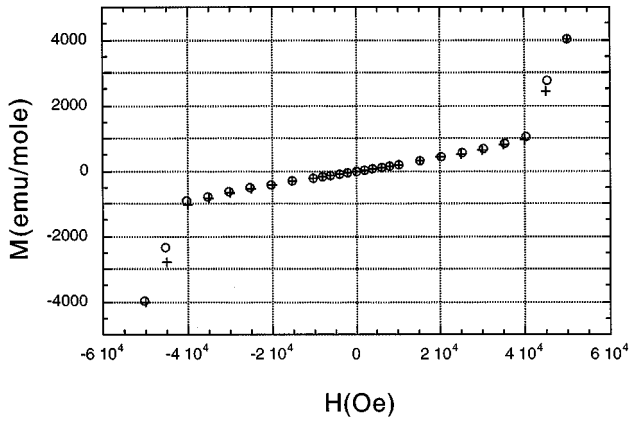

FIG. 7. Magnetization (M) as function of applied magnetic field (H) at $T = 1.7$ K. The open circles are data collected on decreasing field and the plus symbols are data collected on increasing field.

ACKNOWLEDGMENTS

This research was supported in part by the National Science Foundation under Grant DMR 95-20971. We thank Dr. Sarah H. Tolbert for assistance in susceptibility measurements.

REFERENCES

1. D. Blum, J. C. Peuzin, and J. Y. Henry, *Ferroelectrics* **61,** 265 (1984).
2. B. Elouadi and L. Elammari, *Ferroelectrics* **107,** 253 (1990).
3. S. S. Lin and H. S. Weng, *Appl. Catal. A* **105,** 289 (1993).
4. J. Dakka and R. A. Sheldon, Netherland Patent 9,200,968 (1992).
5. G. D. Stucky, M. L. Philips, and T. E. Gier, *Chem. Mater.* **1,** 492 (1989).
6. U. Muller, "Inorganic Structural Chemistry," Wiley, New York 1992.
7. P. Feng, X. Bu, and G. D. Stucky, *J. Solid State Chem.*, in press.
8. X. Bu, P. Feng, and G. D. Stucky, *J. Solid State Chem.***125,** 243–248 (1996).
9. "Inorganic Crystal Structure Database," FIZ Karlsruhe and Gmelin-Institut, 1996.
10. (a) P. Feng, X. Bu, S. H. Tolbert, and G. D. Stucky, *J. Am. Chem. Soc.* **119,** 2497–2504 (1997). (b) X. Bu, P. Feng, T. E. Gier, and G. D. Stucky, submitted.
11. X. Bu, T. E. Gier, and G. D. Stucky, *Acta Crystallogr. C* **52,** 1601–1603 (1996).
12. T. R. Jensen, P. Norby, and P. Stein, *J. Solid State Chem.* **117,** 39–47 (1995).
13. L. Elammari, J. Durand, L. Cot, and B. Elouadi, *Z. Kristallogr.* **180,** 137–140 (1987).
14. C. Gleitzer, *Eur. J. Solid State Inorg. Chem.* **28,** 77–91 (1991).
15. D. Blum, A. Durif, and M. T. Averbuch-Pouchot, *Ferroelectrics* **69,** 283–292 (1986).
16. O. Muller and R. Roy, "The Major Ternary Structural Families," Springer-Verlag, Berlin/New York, 1974.
17. R. L. Carlin, "Magnetochemistry," Springer-Verlag, Berlin/New York, 1986.
18. P. A. Kokkoros and P. J. Rentzeperis, *Acta Crystallogr.* **11,** 361–364 (1958).
19. M. Mipee and G. Giester, *Mineral. Petrol.* **39,** 201–209 (1988).
20. P. C. Burns and F. C. Hawthorne, *Powder Diffr.* **8,** 54–56 (1992).
21. B. R. Rao, *Acta Crystallogr.* **14,** 321–322 (1961).
22. H. Fuess and G. Will, *Z. Anorg. Allg. Chem.* **358,** 125–137 (1968).
23. H. C. Snyman and C. W. F. T. Pistorius, *Z. Kristallogr.* **120,** 317–322 (1964).
24. J. P. Attfield, A. K. Cheetham, D. C. Johnson, and C. C. Torardi, *Inorg. Chem.* **26,** 3379–3383 (1987).
25. J. Morning and E. Kostiner, *J. Solid State Chem.* **61,** 379–383 (1986).
26. J. K. Kabalov, M. A. Simonov, and N. B. Belov, *Dokl. Akad. Nauk SSSR* **216,** 1034–1036 (1974).
27. Y. LePage and G. Donnay, *Can. Mineral.* **15,** 518–521 (1977).